

## OPEN ACCESS

# Bloch–Zener oscillations

To cite this article: B M Breid *et al* 2006 *New J. Phys.* **8** 110

View the [article online](#) for updates and enhancements.

## You may also like

- [Investigation of a wearable piezoelectric-IMU multi-modal sensing system for real-time muscle force estimation](#)  
Yun Lu, Yudong Cao, Yi Chen et al.
- [Unifying system identification and biomechanical formulations for the estimation of muscle, tendon and joint stiffness during human movement](#)  
Christopher P Cop, Gaia Cavallo, Ronald C van 't Veld et al.
- [Energy efficient hopping with Hill-type muscle properties on segmented legs](#)  
Andre Rosendo and Fumiya Iida

## Bloch–Zener oscillations

**B M Breid, D Witthaut and H J Korsch<sup>1</sup>**

FB Physik, Technische Universität Kaiserslautern, D-67653 Kaiserslautern,  
Germany

E-mail: [korsch@physik.uni-kl.de](mailto:korsch@physik.uni-kl.de)

*New Journal of Physics* **8** (2006) 110

Received 30 March 2006

Published 5 July 2006

Online at <http://www.njp.org/>

doi:10.1088/1367-2630/8/7/110

**Abstract.** It is well known that a particle in a periodic potential with an additional constant force performs Bloch oscillations. Modulating every second period of the potential, the original Bloch band splits into two sub-bands. The dynamics of quantum particles shows a coherent superposition of Bloch oscillations and Zener tunnelling between the sub-bands, a Bloch–Zener oscillation. Such a system is modelled by a tight-binding Hamiltonian which is a system of two minibands with an easily controllable gap. The dynamics of the system is investigated by using an algebraic ansatz leading to a differential equation of Whittaker–Hill type. It is shown that the parameters of the system can be tuned to generate a periodic reconstruction of the wave packet and thus of the occupation probability. As an application, the construction of a matter wave beam splitter and a Mach–Zehnder interferometer is briefly discussed.

<sup>1</sup> Author to whom any correspondence should be addressed.

**Contents**

<b>1. Introduction</b>	<b>2</b>
<b>2. Bloch bands in the field-free case</b>	<b>3</b>
<b>3. Spectral properties</b>	<b>5</b>
<b>4. Dynamics</b>	<b>8</b>
4.1. An algebraic ansatz for the time evolution operator . . . . .	8
4.2. Time evolution . . . . .	11
4.3. Bloch–Zener oscillations and reconstruction . . . . .	13
4.4. Oscillating and breathing modes . . . . .	14
4.5. Beam splitters . . . . .	16
<b>5. Conclusion and outlook</b>	<b>17</b>
<b>Acknowledgments</b>	<b>18</b>
<b>Appendix</b>	<b>18</b>
<b>References</b>	<b>19</b>

**1. Introduction**

Since the beginning of quantum mechanics, the dynamics of a particle in a periodic potential has been a subject of fundamental interest. The eigenenergies of such a system form the famous Bloch bands, where the eigenstates are delocalized and exhibit transport [1]. If an additional constant force  $F$  is introduced, the eigenstates become localized. Counterintuitively, transport is dramatically reduced and an oscillatory motion is found, the famous Bloch oscillation. During the last decade, these Bloch oscillations have been experimentally observed for various systems: electrons in semiconductor superlattices [2], cold atoms in optical lattices [3], light pulses in photonic crystals [4, 5] and even mechanical systems may perform Bloch oscillations [6].

If the external field is strong enough, tunnelling between Bloch bands becomes possible, as discussed by Zener [7]. In general, successive Zener tunnelling to even higher bands will lead to decay because the band gaps usually decrease with increasing energy. This decay can be observed as pulsed output for a Bose–Einstein condensate in an optical lattice [8], for electrons in semiconductor superlattices [9] or for light in waveguide arrays [10]. In this case, a description in terms of Wannier–Stark resonances is more suitable than the common Bloch band picture [11].

In order to study and exploit the interplay between Bloch oscillations and Zener tunnelling, a system of at least two bands is needed, which are well separated from all other bands. This is achieved by introducing another weak potential with a doubled period length. Due to this perturbation, the ground band splits into two minibands and Zener tunnelling between the minibands must be taken into account.

In this paper, we discuss the dynamics in such a period-doubled potential within the tight-binding approximation. We assume that the ground state energies of the potential wells are alternately increased or decreased by the additional potential. The Hamiltonian then reads

$$\hat{H} = -\frac{\Delta}{4} \sum_{n=-\infty}^{\infty} (|n\rangle\langle n+1| + |n\rangle\langle n-1|) + \frac{\delta}{2} \sum_{n=-\infty}^{\infty} (-1)^n |n\rangle\langle n| + Fd \sum_{n=-\infty}^{\infty} n |n\rangle\langle n|, \quad (1)$$

where  $|n\rangle$  is the Wannier state localized in the  $n$ th potential well. Furthermore,  $\Delta$  denotes the width of the unperturbed band ( $\delta = 0$ ),  $\delta$  gives the gap between the two minibands at the edge of the Brillouin zone and  $F$  is the external force. For  $\delta = 0$ , this Hamiltonian reduces to the celebrated single-band tight-binding model, which has been studied in great detail (see [12] for a recent review). The period-doubled tight-binding model was introduced for the field-free case  $F = 0$  already in 1988 [13]. The perturbative results with an external field can be found in [14, 15]. Numerical results for an analogous two-miniband system in two spatial dimensions have been reported in [16, 17].

This paper is organized as follows: first of all, we repeat some results for the field-free system  $F = 0$ . The spectral properties for the case  $F \neq 0$  are discussed in section 3, and the dynamics is analysed in detail in section 4. We present an algebraic ansatz for the time evolution operator and analyse the time evolution by general arguments. The interesting case of periodic, i.e. reconstructing, Bloch–Zener oscillations, and thus of reconstructing occupation probabilities, is analysed in detail. These theoretical considerations are illustrated by some numerical results. As an application of Bloch–Zener oscillations, a beam splitting mechanism for matter waves is described and simulated numerically. The possibility of constructing a Mach–Zehnder interferometer based on Bloch–Zener oscillations is briefly discussed.

## 2. Bloch bands in the field-free case

First of all, we discuss the spectrum of the period-doubled Hamiltonian (1) for the field-free case  $F = 0$ , i.e. Bloch bands and Bloch waves. A straightforward calculation yields the dispersion relation

$$E_{\beta,\kappa} = \frac{\gamma}{2}(-1)^{\beta+1} \sqrt{\delta^2 + \Delta^2 \cos^2(\kappa d)}, \quad (2)$$

with the miniband index  $\beta = 0, 1$  and  $\gamma = \text{sgn}(\delta)$ , which is illustrated in figure 1. For  $\delta \neq 0$ , the Bloch band splits into two minibands with band gap  $\delta$ .

The Bloch waves  $|\chi_{\beta,\kappa}\rangle$  of both bands are given by

$$|\chi_{0,\kappa}\rangle = \frac{1}{\sqrt{N_\kappa}} \sum_{n=-\infty}^{\infty} u_\kappa e^{i(2n+1)\kappa d} |2n\rangle + \frac{1}{\sqrt{N_\kappa}} \sum_{n=-\infty}^{\infty} v_\kappa e^{i(2n+2)\kappa d} |2n+1\rangle, \quad (3)$$

$$|\chi_{1,\kappa}\rangle = \frac{1}{\sqrt{N_\kappa}} \sum_{n=-\infty}^{\infty} v_\kappa e^{i(2n)\kappa d} |2n\rangle - \frac{1}{\sqrt{N_\kappa}} \sum_{n=-\infty}^{\infty} u_\kappa e^{i(2n+1)\kappa d} |2n+1\rangle, \quad (4)$$

with normalization constant  $N_\kappa = \pi(u_\kappa^2 + v_\kappa^2)/d$  and coefficients

$$u_\kappa = \Delta \cos(\kappa d) \quad \text{and} \quad v_\kappa = \delta + \gamma \sqrt{\delta^2 + \Delta^2 \cos^2(\kappa d)}. \quad (5)$$

In the Bloch basis, the time-independent Schrödinger equation with Hamiltonian (1) reads

$$E \langle \chi_{0,\kappa} | \Psi \rangle = E_{0,\kappa} \langle \chi_{0,\kappa} | \Psi \rangle + iF \frac{\partial}{\partial \kappa} \langle \chi_{0,\kappa} | \Psi \rangle - Fd \langle \chi_{0,\kappa} | \Psi \rangle - M_\kappa \langle \chi_{1,\kappa} | \Psi \rangle, \quad (6)$$

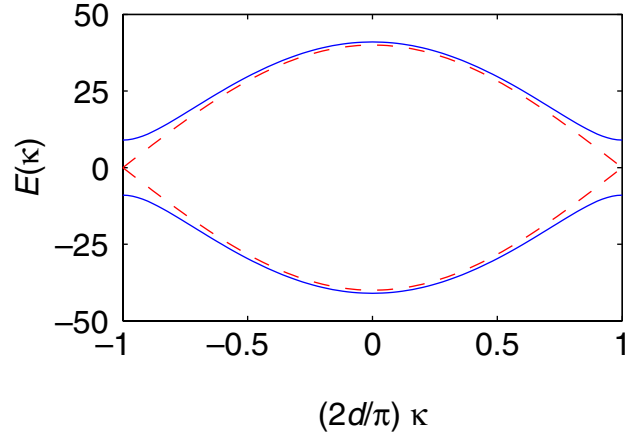


**Figure 1.** Dispersion relation of the double-periodic system in the reduced Brillouin zone for  $\Delta = 80$ . The Bloch bands for  $\delta = 0$  (dashed curve) split into two minibands with gap  $\delta$  (solid lines for  $\delta = 18$ ).

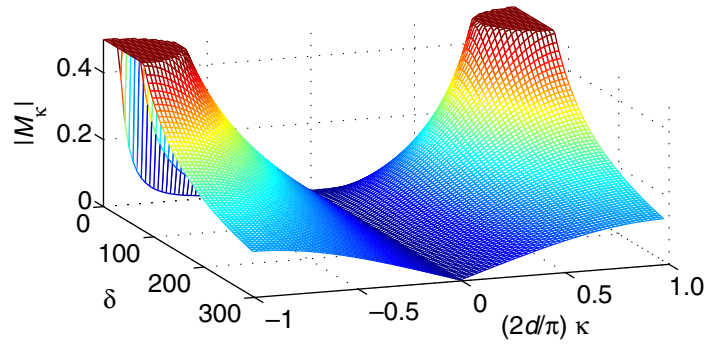


**Figure 2.** Absolute value of the reduced transition matrix element  $|M_\kappa|$  for  $\Delta = 80$  and  $dF = 1$ . The range  $|M_\kappa| > 0.5$  has been cut off to increase the visibility.

$$E\langle\chi_{1,\kappa}|\Psi\rangle = E_{1,\kappa}\langle\chi_{1,\kappa}|\Psi\rangle + iF\frac{\partial}{\partial\kappa}\langle\chi_{1,\kappa}|\Psi\rangle + M_\kappa\langle\chi_{0,\kappa}|\Psi\rangle, \quad (7)$$

where the coupling of the two bands is given by the transition matrix element

$$\langle\chi_{1,\kappa'}|\hat{H}_{ZB}|\chi_{0,\kappa}\rangle = M_\kappa\delta_{\frac{\pi}{d}}(\kappa - \kappa'), \quad (8)$$

with the reduced matrix element

$$M_\kappa = iF\frac{\left(\frac{\partial}{\partial\kappa}u_\kappa\right)v_\kappa - \left(\frac{\partial}{\partial\kappa}v_\kappa\right)u_\kappa}{u_\kappa^2 + v_\kappa^2}e^{i\kappa d} = -\frac{iFd\Delta\delta\sin(\kappa d)e^{i\kappa d}}{2\delta^2 + 2\Delta^2\cos^2(\kappa d)}, \quad (9)$$

(cf [14]). The modulus of  $M_\kappa$  is shown in figure 2.

Obviously, the band transitions mainly take place at the edge of the Brillouin zone, and because of the delta-function in (8), only direct interband transitions are possible.

### 3. Spectral properties

We now discuss the spectrum of the two-miniband Hamiltonian (1) with an external field. The spectrum of the single-band Wannier–Stark Hamiltonian ( $\delta = 0$ ) consists of a ladder of equally spaced eigenvalues—the Wannier–Stark ladder. Note that beyond the single-band tight-binding approximation, these eigenstates become resonances embedded into a continuum (see [11] for a review). In the case of two minibands,  $\delta \neq 0$ , the spectrum consists of two ladders with an offset in between, as will be shown below. Furthermore, the dependence of the offset on the system parameters will be discussed in detail. Certain aspects of the spectrum were previously discussed in [14].

To keep the notation simple, we introduce the translation operator

$$\hat{T}_m = \sum_{n=-\infty}^{\infty} |n-m\rangle\langle n|, \quad (10)$$

and an operator  $\hat{G}$  that causes the inversion of the sign of  $\delta$  in all following terms. They fulfil the following commutation relations

$$[\hat{T}_m, \hat{H}] = \frac{\delta}{2} \sum_{n=-\infty}^{\infty} (-1)^n [1 - (-1)^m] |n-m\rangle\langle n| + Fd \sum_{n=-\infty}^{\infty} m |n-m\rangle\langle n|, \quad (11)$$

$$[\hat{G}, \hat{H}] = -\delta \sum_{n=-\infty}^{\infty} (-1)^n |n\rangle\langle n| \hat{G} \quad \text{and} \quad [\hat{T}_m, \hat{G}] = 0. \quad (12)$$

An eigenvector  $|\Psi\rangle$  of  $\hat{H}$  with the eigenvalue  $E(\delta, \Delta, Fd)$ ,

$$\hat{H}|\Psi\rangle = E(\delta, \Delta, Fd)|\Psi\rangle, \quad (13)$$

satisfies

$$\hat{H}\{\hat{T}_{2l}|\Psi\rangle\} = \{E(\delta, \Delta, Fd) - 2ldF\}\{\hat{T}_{2l}|\Psi\rangle\}, \quad (14)$$

$$\hat{H}\{\hat{T}_{2l+1}\hat{G}|\Psi\rangle\} = \{E(-\delta, \Delta, Fd) - (2l+1)Fd\}\{\hat{T}_{2l+1}\hat{G}|\Psi\rangle\}. \quad (15)$$

Thus the applications of the operators  $\hat{T}_{2l}$  and  $\hat{T}_{2l+1}\hat{G}$  to the eigenvector  $|\Psi\rangle$  yield two ladders of eigenvectors

$$\hat{H}|\Psi_{\alpha,n}\rangle = E_{\alpha,n}|\Psi_{\alpha,n}\rangle \quad \text{with } \alpha = 0, 1, \quad (16)$$

defined by

$$|\Psi_{0,n}\rangle = \hat{T}_{-2n}|\Psi\rangle \quad \text{and} \quad |\Psi_{1,n}\rangle = \hat{G}\hat{T}_{-(2n+1)}|\Psi\rangle, \quad (17)$$

with equidistant eigenenergies

$$E_{0,n} = E(\delta, \Delta, Fd) + 2ndF, \quad (18)$$

$$E_{1,n} = E(-\delta, \Delta, Fd) + (2n + 1)dF. \quad (19)$$

Thus the spectrum of the Hamiltonian (1) consists of two energy ladders with equal spacings and an offset given by  $E(\delta, \Delta, Fd)$ . Furthermore, it can be shown that there are not more than two different energy ladders (see appendix). The eigenvectors  $|\Psi_{\alpha,n}\rangle$  are displaced by  $2n$  lattice periods with respect to  $|\Psi_{\alpha,0}\rangle$ , where  $\alpha$  labels the two ladders.

The dependence of  $E(\delta, \Delta, Fd)$  on the system parameters  $\delta$ ,  $\Delta$  and  $Fd$  shows several interesting symmetries. In the case  $\delta = 0$ , it is well known that for all values of  $\Delta$  and  $Fd$  we can choose  $E(0, \Delta, Fd) = 0$  [12]. In the case  $\delta \neq 0$ , it can be shown that  $E(-\delta, \Delta, Fd) = -E(\delta, \Delta, Fd)$  holds, as well as  $E(\delta, -\Delta, Fd) = E(\delta, \Delta, Fd)$ . The proofs of these relations are quite similar and only one of them is given here. We consider the operator  $\hat{X}$  defined by

$$\hat{X} = \sum_{n=-\infty}^{\infty} |-n\rangle\langle n|(-1)^n, \quad (20)$$

which fulfils the relation

$$\hat{X}\hat{H}(\delta, \Delta, Fd) = -\hat{H}(-\delta, \Delta, Fd)\hat{X}. \quad (21)$$

Applying  $-\hat{X}$  to equation (16) yields

$$\begin{aligned} -E_{\alpha,n}(\delta, \Delta, Fd)\{\hat{X}|\Psi_{\alpha,n}\rangle\} &= \hat{H}(-\delta, \Delta, Fd)\{\hat{X}|\Psi_{\alpha,n}\rangle\} \\ &=: E_{\alpha',n'}(-\delta, \Delta, Fd)\{\hat{X}|\Psi_{\alpha,n}\rangle\}. \end{aligned} \quad (22)$$

This means that the whole spectrum is antisymmetric by means of

$$-E_{\alpha,n}(\delta, \Delta, Fd) = E_{\alpha',n'}(-\delta, \Delta, Fd). \quad (23)$$

To simplify the following argumentation, we consider without loss of generality the whole spectrum  $\mathcal{S}$  modulo  $2dF$ . Thus we get

$$\mathcal{S} = \{E(\delta, \Delta, Fd), E(-\delta, \Delta, Fd) + dF\}_{\text{mod } 2dF}. \quad (24)$$

For  $-\delta$ , the spectrum therefore reads

$$\mathcal{S} = \{E(-\delta, \Delta, Fd), E(\delta, \Delta, Fd) + dF\}_{\text{mod } 2dF}. \quad (25)$$

By equation (23), this must be equal to

$$\begin{aligned} \mathcal{S} &= \{-E(\delta, \Delta, Fd), -E(-\delta, \Delta, Fd) - dF\}_{\text{mod } 2dF} \\ &= \{-E(\delta, \Delta, Fd), -E(-\delta, \Delta, Fd) + dF\}_{\text{mod } 2dF}. \end{aligned} \quad (26)$$

From the equivalence of the equations (25) and (26), it follows that

$$E(-\delta, \Delta, Fd) = -E(\delta, \Delta, Fd). \quad (27)$$

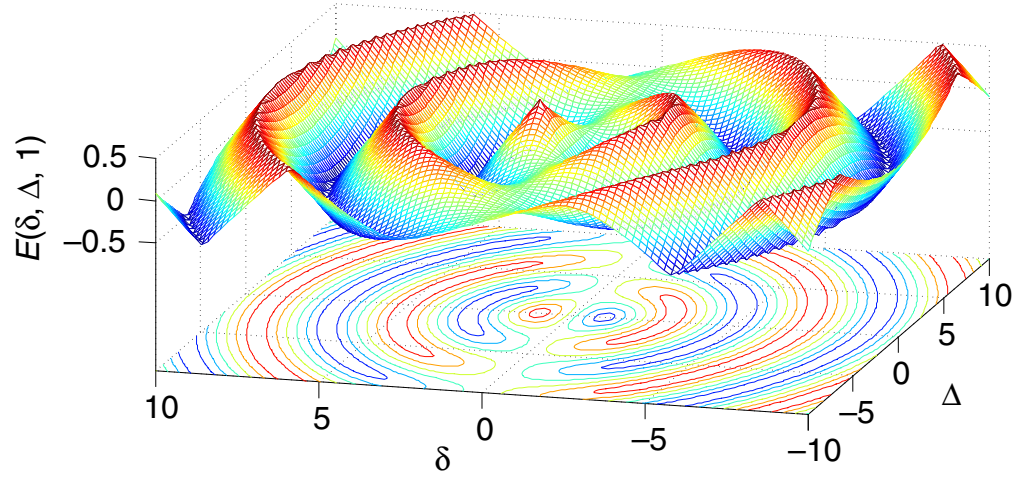


**Figure 3.** Alternating energy shift  $E(\delta, \Delta, 1)$  versus  $\delta$  and  $\Delta$  for  $Fd = 1$ .

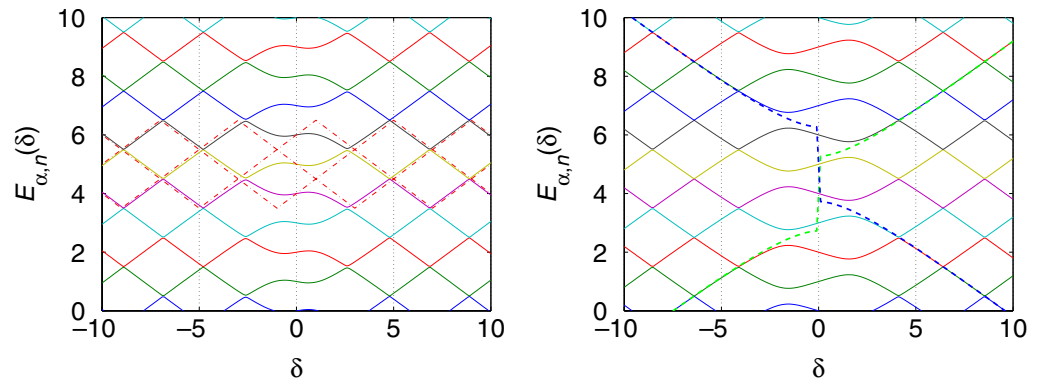


**Figure 4.** Spectrum  $E_{\alpha,n}(\delta)$  of the Hamiltonian (1) for  $Fd = 1$  (solid lines). The left-hand side shows the case  $\Delta = 2$ , where  $\Delta = 0$  is given as reference (dashed line). Note the avoided crossings of the energy levels. The right-hand side shows the spectrum for  $\Delta = 4$ . Here, two rungs of different energy ladders calculated with the approximation  $M_\kappa \approx 0$  (dashed lines, cf equation (30)) are shown for comparison.

Numerical results for the energy offset  $E(\delta, \Delta, 1)$  and the energy ladders  $E_{\alpha,n}(\delta, \Delta, 1)$  are shown in figures 3 and 4. In all examples, we consider only the case  $Fd = 1$ , as all other cases can be reduced to it by a simple scaling

$$E_{\alpha,n}(\delta, \Delta, Fd) = dFE_{\alpha,n}\left(\frac{\delta}{Fd}, \frac{\Delta}{Fd}, 1\right), \quad (28)$$

which directly follows from a rescaling of the Hamiltonian  $\hat{H}$  by  $Fd$ .



In certain limits, one can easily derive some analytic approximations for the ladder offset  $E(\delta, \Delta, Fd)$ :

- (i) For  $\delta \gg \Delta$ , the two minibands are well separated energetically, so that their coupling can be neglected. Hence one sets  $M_\kappa \approx 0$  in the equations (6) and (7). The energy shift is then given by

$$E(\delta, \Delta, Fd) = \frac{\gamma}{\pi} \sqrt{\delta^2 + \Delta^2} I\left(\frac{\pi}{2}, \sqrt{\frac{\Delta^2}{\delta^2 + \Delta^2}}\right), \quad (29)$$

$$= \frac{\gamma}{\pi} \int_0^{\pi/2} \sqrt{\delta^2 + \Delta^2 \cos^2 y} dy, \quad (30)$$

(compare [14]) with  $\gamma = \text{sgn}(\delta)$ . Here,  $I$  denotes the incomplete elliptic integral of the second kind [18]. This approximation is compared to the numerical results in figure 4.

- (ii) For small  $\delta$  perturbation theory can be done, which yields

$$E(\delta, \Delta, Fd) = \frac{\delta}{2} J_0\left(\frac{\Delta}{Fd}\right), \quad (31)$$

where  $J_0$  denotes the ordinary Bessel function.

The zeros of  $E(\delta, 0, 1)$  are  $\delta = 0, \pm 2, \pm 4, \dots$  (see figure 3), whereas the zeros of  $E(\delta, \Delta, 1)$  for very small  $\delta$  are given by the zeros of  $J_0(\Delta)$  (see equation (31)) which are  $\Delta \approx n\pi$  for large  $\Delta$ . These relations indicate that the characteristic structure of the energy shift looks similar for large  $\Delta$  and large  $\delta$ . In figure 4, one clearly sees the asymmetry of  $E(\delta, \Delta, 1)$  with respect to  $\delta$ . Avoided crossings appear in the typical case of  $\Delta \neq 0$ .

## 4. Dynamics

### 4.1. An algebraic ansatz for the time evolution operator

In this section, we derive some general results for the time evolution operator  $\hat{U}$ . The single-band system  $\delta = 0$  can be treated conveniently within a Lie-algebraic approach [19]. To simplify notation, we rewrite the Hamiltonian (1) using the operators

$$\hat{N} = \sum_{n=-\infty}^{\infty} n |n\rangle \langle n|, \quad \hat{L} = \sum_{n=-\infty}^{\infty} (-1)^n |n\rangle \langle n| = (-1)^{\hat{N}}, \quad (32)$$

$$\hat{K} = \sum_{n=-\infty}^{\infty} |n-1\rangle \langle n| \quad \text{and} \quad \hat{K}^\dagger = \sum_{n=-\infty}^{\infty} |n+1\rangle \langle n|. \quad (33)$$

These operators fulfil the commutator relations

$$[\hat{K}, \hat{N}] = \hat{K}, \quad [\hat{K}^\dagger, \hat{N}] = -\hat{K}^\dagger, \quad [\hat{K}^\dagger, \hat{K}] = 0, \quad (34)$$

and

$$[\hat{L}, \hat{N}] = 0, \quad [\hat{K}^\dagger, \hat{L}] = 2\hat{K}^\dagger \hat{L}, \quad [\hat{K}, \hat{L}] = 2\hat{K} \hat{L}. \quad (35)$$

From the commutator relations of  $\hat{K}^\dagger$ ,  $\hat{K}$  and  $\hat{L}$ , one concludes that for any function  $\hat{f}$  of the shift operators alone, one has

$$\hat{f}(\hat{K}, \hat{K}^\dagger)\hat{L} = \hat{L}\hat{f}(-\hat{K}, -\hat{K}^\dagger). \quad (36)$$

The Schrödinger equation for the time evolution operator  $\hat{U}$ , then reads

$$i\hbar \frac{\partial}{\partial t} \hat{U} = \left[ -\frac{\Delta}{4}(\hat{K} + \hat{K}^\dagger) + \frac{\delta}{2}\hat{L} + Fd\hat{N} \right] \hat{U}. \quad (37)$$

In analogy to the single-band system [19], we make the ansatz

$$\hat{U} = e^{-iC(t)\hat{N}} [\hat{A}(\hat{K}, \hat{K}^\dagger, t) + \hat{L}\hat{B}(\hat{K}, \hat{K}^\dagger, t)], \quad (38)$$

where  $C(t)$ ,  $\hat{A}(\hat{K}, \hat{K}^\dagger, t)$  and  $\hat{B}(\hat{K}, \hat{K}^\dagger, t)$  are yet unknown functions or operators. To abbreviate the notation we do not write the arguments of the operator valued functions  $\hat{A}(t)$  and  $\hat{B}(t)$  in the following explicitly. Substituting equation (38) into (37) leads to

$$\begin{aligned} \hbar \dot{C}(t)\hat{N}e^{-iC(t)\hat{N}}[\hat{A}(t) + \hat{L}\hat{B}(t)] + i\hbar e^{-iC(t)\hat{N}}[\dot{\hat{A}}(t) + \hat{L}\dot{\hat{B}}(t)] \\ = Fd\hat{N}e^{-iC(t)\hat{N}}[\hat{A}(t) + \hat{L}\hat{B}(t)] - \frac{\Delta}{4}\hat{K}e^{-iC(t)\hat{N}}[\hat{A}(t) \\ + \hat{L}\hat{B}(t)] - \frac{\Delta}{4}\hat{K}^\dagger e^{-iC(t)\hat{N}}[\hat{A}(t) + \hat{L}\hat{B}(t)] + \frac{\delta}{2}\hat{L}e^{-iC(t)\hat{N}}[\hat{A}(t) + \hat{L}\hat{B}(t)]. \end{aligned} \quad (39)$$

Here and in the following, the dot denotes the derivative with respect to the time  $t$ . The first term of the left- and the right-hand side of equation (39) cancel each other if

$$\hbar \dot{C}(t) = Fd \implies C(t) = \frac{d}{\hbar} \int_0^t F(\tau) d\tau. \quad (40)$$

The remaining terms in equation (39) can be simplified by multiplying with  $e^{iC(t)\hat{N}}$  from the left and using the relations

$$e^{iC(t)\hat{N}}\hat{K}e^{-iC(t)\hat{N}} = e^{-iC(t)}\hat{K}, \quad (41)$$

$$e^{iC(t)\hat{N}}\hat{K}^\dagger e^{-iC(t)\hat{N}} = e^{iC(t)}\hat{K}^\dagger, \quad (42)$$

which follow from the Baker–Hausdorff formula

$$e^{z\hat{Y}}\hat{X}e^{-z\hat{Y}} = \hat{X} + z[\hat{Y}, \hat{X}] + \frac{z^2}{2!}[\hat{Y}, [\hat{Y}, \hat{X}]] + \frac{z^3}{3!}[\hat{Y}, [\hat{Y}, [\hat{Y}, \hat{X}]]] + \dots \quad (43)$$

Since  $\hat{L}$  and  $\hat{N}$  commute and  $\hat{L}\hat{L} = \mathbb{1}$ , one finally arrives at

$$\begin{aligned} \hat{L} \left( i\hbar \dot{\hat{B}}(t) - \frac{\Delta}{4}e^{-iC(t)}\hat{K}\hat{B}(t) - \frac{\Delta}{4}e^{iC(t)}\hat{K}^\dagger\hat{B}(t) - \frac{\delta}{2}\hat{A}(t) \right) \\ = - \left( i\hbar \dot{\hat{A}}(t) + \frac{\Delta}{4}e^{-iC(t)}\hat{K}\hat{A}(t) + \frac{\Delta}{4}e^{iC(t)}\hat{K}^\dagger\hat{A}(t) - \frac{\delta}{2}\hat{B}(t) \right). \end{aligned} \quad (44)$$

Obviously, this equation is fulfilled if each bracket is zero. The result is two coupled differential equations

$$\dot{\hat{A}}(t) = i\frac{\Delta}{4\hbar}(e^{-iC(t)}\hat{K} + e^{iC(t)}\hat{K}^\dagger)\hat{A}(t) - i\frac{\delta}{2\hbar}\hat{B}(t), \quad (45)$$

$$\dot{\hat{B}}(t) = -i\frac{\Delta}{4\hbar}(e^{-iC(t)}\hat{K} + e^{iC(t)}\hat{K}^\dagger)\hat{B}(t) - i\frac{\delta}{2\hbar}\hat{A}(t), \quad (46)$$

that only depend on the commuting operators  $\hat{K}$  and  $\hat{K}^\dagger$ . With the initial condition  $\hat{U}(0) = \mathbb{1}$  and the equations (38), (45) and (46), we conclude

$$\hat{A}(0) = \mathbb{1}, \quad \dot{\hat{A}}(0) = i\frac{\Delta}{4\hbar}(\hat{K} + \hat{K}^\dagger), \quad (47)$$

$$\hat{B}(0) = 0, \quad \dot{\hat{B}}(0) = -i\frac{\delta}{2\hbar}. \quad (48)$$

Without loss of generality, we continue with the representation of  $\hat{K}$  and  $\hat{K}^\dagger$  in the  $\kappa$ -basis of the single-band system

$$|\kappa\rangle = \sqrt{\frac{d}{2\pi}} \sum_{n=-\infty}^{\infty} e^{in\kappa d} |n\rangle, \quad (49)$$

where the operators are diagonal with respect to the quasi-momentum  $\kappa$

$$\langle\kappa'|\hat{K}|\kappa\rangle = e^{i\kappa d} \delta_{\frac{2\pi}{d}}(\kappa - \kappa') \quad \text{and} \quad \langle\kappa'|\hat{K}^\dagger|\kappa\rangle = e^{-i\kappa d} \delta_{\frac{2\pi}{d}}(\kappa - \kappa'), \quad (50)$$

with the  $(2\pi/d)$ -periodic delta function  $\delta_{\frac{2\pi}{d}}$ . The operators  $\hat{A}(\hat{K}, \hat{K}^\dagger, t)$  and  $\hat{B}(\hat{K}, \hat{K}^\dagger, t)$  in the  $\kappa$ -basis are denoted by  $A_\kappa(t)$  and  $B_\kappa(t)$ , which leads to the following system of ordinary differential equations

$$\dot{A}_\kappa(t) = i\frac{\Delta}{2\hbar} \cos[\kappa d - C(t)] A_\kappa(t) - i\frac{\delta}{2\hbar} B_\kappa(t), \quad (51)$$

$$\dot{B}_\kappa(t) = -i\frac{\Delta}{2\hbar} \cos[\kappa d - C(t)] B_\kappa(t) - i\frac{\delta}{2\hbar} A_\kappa(t). \quad (52)$$

From now on, we consider the case of a constant force  $C(t) = dFt/\hbar$ . By substituting

$$x = \kappa d - \frac{dFt}{\hbar} \quad \text{and} \quad \frac{\partial}{\partial t} = -\frac{dF}{\hbar} \frac{\partial}{\partial x}, \quad (53)$$

one obtains

$$A'_\kappa(x) = -i\frac{\Delta}{2dF} \cos(x) A_\kappa(x) + i\frac{\delta}{2dF} B_\kappa(x), \quad (54)$$

$$B'_\kappa(x) = i \frac{\Delta}{2dF} \cos(x) B_\kappa(x) + i \frac{\delta}{2dF} A_\kappa(x), \quad (55)$$

where the prime denotes differentiation with respect to  $x$ . Differentiating again with respect to  $x$  decouples these equations with the result

$$A''_\kappa(x) + \left[ \left( \frac{\delta}{2dF} \right)^2 - i \left( \frac{\Delta}{2dF} \right) \sin x + \left( \frac{\Delta}{2dF} \right)^2 \cos^2 x \right] A_\kappa(x) = 0, \quad (56)$$

$$B''_\kappa(x) + \left[ \left( \frac{\delta}{2dF} \right)^2 + i \left( \frac{\Delta}{2dF} \right) \sin x + \left( \frac{\Delta}{2dF} \right)^2 \cos^2 x \right] B_\kappa(x) = 0. \quad (57)$$

Both equations are differential equations of Whittaker–Hill type, as described, e.g., in [20]. A solution of the equations (56), (57) in closed form is only known in the cases  $\delta = 0$  or  $\Delta = 0$ . The equations (51) and (52) can of course be solved in the case  $F = 0$ . There always exists a solution of the differential equations (56), (57) which justifies the ansatz (38), even if we cannot construct such a solution in closed form.

#### 4.2. Time evolution

A wave packet whose dynamics is governed by the double-periodic Hamiltonian (1) is expected to show both Bloch oscillations and Zener tunnelling simultaneously. The tunnelling rate at the edge of the Brillouin zone is approximately given by the famous Landau–Zener formula [21, 22]

$$P \approx e^{-\frac{\pi \delta^2}{2d|F\Delta|}}. \quad (58)$$

In this section, we study Bloch–Zener oscillations, a coherent superposition of Bloch oscillations and Zener tunnelling. Let  $|\Psi_{\alpha,n}\rangle$  be the eigenfunctions of the Hamiltonian (1), called Wannier–Stark functions, as introduced in section 3. The index  $\alpha = 0, 1$  labels the two energy ladders. We expand the Wannier–Stark functions in the  $\kappa$ -basis,

$$|\Psi_{\alpha,n}\rangle = \int_{-\frac{\pi}{2d}}^{\frac{\pi}{2d}} a_{\alpha,n}(\kappa) |\chi_{0,\kappa}\rangle d\kappa + \int_{-\frac{\pi}{2d}}^{\frac{\pi}{2d}} b_{\alpha,n}(\kappa) |\chi_{1,\kappa}\rangle d\kappa, \quad (59)$$

with unknown coefficients  $a_{\alpha,n}(\kappa)$  and  $b_{\alpha,n}(\kappa)$ . According to equation (17), the Wannier–Stark functions with different site indices  $n$  are related by the translation operator  $\hat{T}_m$  (see equation (8)). The Bloch waves of the two band system defined by the equations (3), (4) obey the relations

$$\hat{T}_{-2n} |\chi_{\beta,\kappa}\rangle = e^{-i2n\kappa d} |\chi_{\beta,\kappa}\rangle. \quad (60)$$

Thus the Wannier–Stark functions (59) can be written as

$$|\Psi_{\alpha,n}\rangle = \int_{-\frac{\pi}{2d}}^{\frac{\pi}{2d}} a_{\alpha,0}(\kappa) e^{-i2n\kappa d} |\chi_{0,\kappa}\rangle d\kappa + \int_{-\frac{\pi}{2d}}^{\frac{\pi}{2d}} b_{\alpha,0}(\kappa) e^{-i2n\kappa d} |\chi_{1,\kappa}\rangle d\kappa, \quad (61)$$

with projections on to the Bloch states

$$\langle \chi_{0,\kappa} | \Psi_{\alpha,n} \rangle = a_{\alpha,0}(\kappa) e^{-i2n\kappa d} \quad \text{and} \quad \langle \chi_{1,\kappa} | \Psi_{\alpha,n} \rangle = b_{\alpha,0}(\kappa) e^{-i2n\kappa d}. \quad (62)$$

The time evolution of an arbitrary initial state  $|\psi(0)\rangle$  can now be calculated in the Wannier–Stark basis. Expanding the initial state in the Wannier–Stark basis,

$$|\psi(0)\rangle = \sum_n c_{0,n} |\Psi_{0,n}\rangle + \sum_n c_{1,n} |\Psi_{1,n}\rangle, \quad (63)$$

the dynamics of  $|\psi\rangle$  is given by

$$|\psi(t)\rangle = \sum_n c_{0,n} e^{-\frac{i}{\hbar} E_{0,n} t} |\Psi_{0,n}\rangle + \sum_n c_{1,n} e^{-\frac{i}{\hbar} E_{1,n} t} |\Psi_{1,n}\rangle. \quad (64)$$

The contributions of the Bloch bands are obtained by projecting on to  $|\chi_{\alpha,\kappa}\rangle$ , which yields

$$\langle \chi_{0,\kappa} | \Psi(t) \rangle = \sum_n c_{0,n} e^{-\frac{i}{\hbar} (2ndF + E_0)t} a_{0,0}(\kappa) e^{-i2n\kappa d} + \sum_n c_{1,n} e^{-\frac{i}{\hbar} (2ndF + dF - E_0)t} a_{1,0}(\kappa) e^{-i2n\kappa d}, \quad (65)$$

$$\langle \chi_{1,\kappa} | \Psi(t) \rangle = \sum_n c_{0,n} e^{-\frac{i}{\hbar} (2ndF + E_0)t} b_{0,0}(\kappa) e^{-i2n\kappa d} + \sum_n c_{1,n} e^{-\frac{i}{\hbar} (2ndF + dF - E_0)t} b_{1,0}(\kappa) e^{-i2n\kappa d}, \quad (66)$$

where the eigenenergies (18), (19) have been inserted and the notation has been simplified by defining

$$E_0 = E(\delta, \Delta, Fd). \quad (67)$$

One observes that two Fourier series appear for the two ladders  $\alpha = 0, 1$ ,

$$C_\alpha \left( \kappa + \frac{Ft}{\hbar} \right) = \sum_n c_{\alpha,n} e^{-i2nd(\kappa + \frac{Ft}{\hbar})}, \quad (68)$$

which are  $\pi/d$ -periodic. Thus the time evolution can be written as

$$\langle \chi_{0,\kappa} | \Psi(t) \rangle = e^{-\frac{i}{\hbar} E_0 t} \left[ a_{0,0}(\kappa) C_0 \left( \kappa + \frac{Ft}{\hbar} \right) + a_{1,0}(\kappa) e^{-\frac{i}{\hbar} (dF - 2E_0)t} C_1 \left( \kappa + \frac{Ft}{\hbar} \right) \right], \quad (69)$$

$$\langle \chi_{1,\kappa} | \Psi(t) \rangle = e^{-\frac{i}{\hbar} E_0 t} \left[ b_{0,0}(\kappa) C_0 \left( \kappa + \frac{Ft}{\hbar} \right) + b_{1,0}(\kappa) e^{-\frac{i}{\hbar} (dF - 2E_0)t} C_1 \left( \kappa + \frac{Ft}{\hbar} \right) \right]. \quad (70)$$

This structure of the dynamics produces some interesting effects discussed in the following section.

### 4.3. Bloch–Zener oscillations and reconstruction

The dynamics of the two band system is characterized by two periods. The functions  $C_0$  and  $C_1$  are reconstructed at multiples of

$$T_1 = \frac{\pi\hbar}{dF}, \quad (71)$$

whereas the exponential function  $e^{-\frac{i}{\hbar}(dF-2E_0)t}$  has a period of

$$T_2 = \frac{2\pi\hbar}{dF - 2E_0}. \quad (72)$$

The period  $T_1$  is just half of the Bloch time  $T_B = (2\pi\hbar)/(dF)$  for the single-band system,  $\delta = 0$ , which reflects the double periodicity of the two band model. In the case of a wavefunction confined to a single energy ladder, one of the functions  $C_0$  and  $C_1$  is zero for all times  $t$  and the initial state is reconstructed up to a global phase after a period  $T_1$ , which is just an ordinary Bloch oscillation.

In general, the functions (69) and (70) reconstruct up to a global phase if the two periods  $T_1$  and  $T_2$  are commensurate,

$$\frac{T_2}{T_1} = \frac{2dF}{dF - 2E_0} = \frac{r}{s} \quad \text{with } r, s \in \mathbb{N}. \quad (73)$$

The reconstruction takes place at integer multiples of the Bloch–Zener time

$$T_{BZ} = sT_2 = rT_1. \quad (74)$$

Examples of such reconstructing Bloch–Zener oscillations are shown in the next section. Furthermore, we can calculate the dynamics of the occupation probability at multiples of  $T_1$  by the aid of the equations (69), (70), which yields

$$\int_{-\frac{\pi}{2d}}^{\frac{\pi}{2d}} |\langle \chi_{0,\kappa} | \Psi(nT_1) \rangle|^2 d\kappa = X + Y \cos\left(\frac{dF - 2E_0}{dF} \pi n + \varphi\right), \quad (75)$$

$$\int_{-\frac{\pi}{2d}}^{\frac{\pi}{2d}} |\langle \chi_{1,\kappa} | \Psi(nT_1) \rangle|^2 d\kappa = 1 - \left[ X + Y \cos\left(\frac{dF - 2E_0}{dF} \pi n + \varphi\right) \right], \quad (76)$$

where  $X$  and  $Y$  are real positive numbers. In the commensurate case (73), we find

$$\int_{-\frac{\pi}{2d}}^{\frac{\pi}{2d}} |\langle \chi_{0,\kappa} | \Psi(nT_1) \rangle|^2 d\kappa = X + Y \cos\left(2\pi \frac{s}{r} n + \varphi\right), \quad (77)$$

$$\int_{-\frac{\pi}{2d}}^{\frac{\pi}{2d}} |\langle \chi_{1,\kappa} | \Psi(nT_1) \rangle|^2 d\kappa = 1 - \left[ X + Y \cos\left(2\pi \frac{s}{r} n + \varphi\right) \right], \quad (78)$$

where one recognizes the reconstruction at integer multiples of  $T_{BZ}$ . In the case of incommensurate periods  $T_2$  and  $T_1$ , we obtain  $\varphi = 0$  whenever only one of the bands is occupied at the beginning. Otherwise one of the occupation probabilities would become greater than one for some  $n$ , while the other one would become negative.

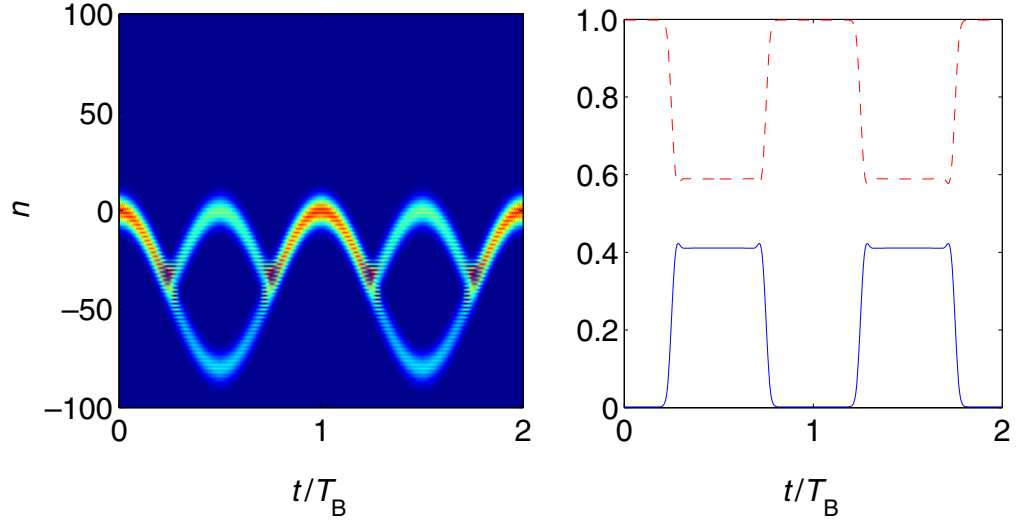


**Figure 5.** Dynamics of an oscillating Bloch–Zener mode. The left-hand side shows  $|\psi|^2$  versus ‘space’ (lattice site  $n$ ) and time. The right-hand side shows the occupation probability of the lower miniband (dashed red line) and the upper band (solid blue line) versus time. The parameters are  $\Delta = 80$ ,  $dF = 1$  and  $\delta = 6.734$ .

#### 4.4. Oscillating and breathing modes

The reconstructing Bloch–Zener oscillations discussed in the preceding section will be illustrated by some numerical calculations. The dynamics of a so-called oscillatory mode is shown in figure 5. Because of the strong localization of the Wannier functions, this resembles closely the behaviour in real space. The initial state is chosen as a broad Gaussian distribution in the Wannier representation, namely  $\sim e^{-n^2/100}$ . By the choice of the parameters, we have  $E_0 = 0$  and we obtain a reconstruction at integer multiples of the Bloch time  $T_{\text{BZ}} = T_{\text{B}}$ . Here and in the following, we take the Bloch time  $T_{\text{B}} = 2\pi\hbar/dF = 2T_1$  of the single-band system  $\delta = 0$  as the reference timescale. Many other reconstruction times  $T_{\text{BZ}}$  can obviously be adjusted in this way. The edge of the Brillouin zone is reached at multiples of  $T_1 = T_{\text{B}}/2$ , where the Bloch bands are close together and the probability for a band transition reaches a maximum.

When  $(dF - 2E_0/dF\pi)$  is close to  $2\pi$ , the cosine in equations (77) and (78) changes very slightly after each period  $T_1$ , which illustrates the cosine-like behaviour of the occupation probability very clearly. This is shown in figure 6 for an oscillatory mode with the same initial condition as above. By the choice of the parameters  $\Delta$ ,  $dF$  and  $\delta$ , we get  $E_0 = -0.5178$  and hence

$$\frac{T_2}{T_1} = \frac{56}{57}. \quad (79)$$

Thus we get a reconstruction at multiples of  $T_{\text{BZ}} = 28T_{\text{B}}$ . The slowly varying oscillation of the occupation between the Bloch bands is similar to the Rabi oscillations for a two level system.

Let us now consider a wave packet that is initially located at a single site (see figure 7). In the case of a single-band system ( $\delta = 0$ ), one finds a breathing behaviour: the width of the wave packet oscillates strongly, while its position remains constant [12]. The parameters are

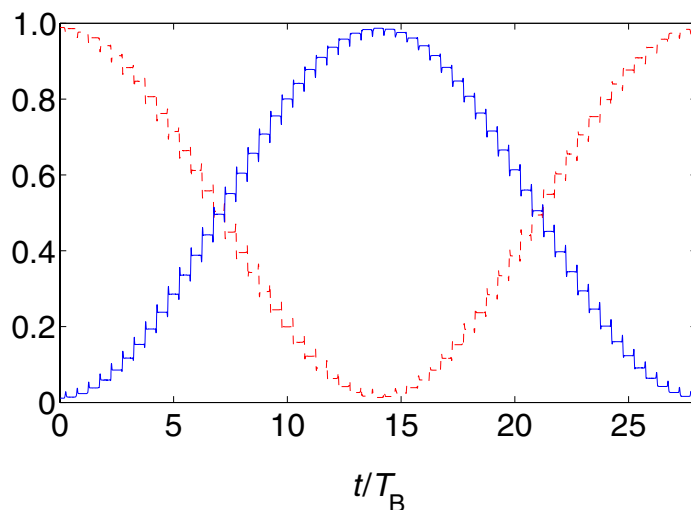


**Figure 6.** Occupation probability of the lower miniband (dashed red line) and the upper band (solid blue line) for an oscillatory mode versus time. The parameters are  $\Delta = 80$ ,  $dF = 1$  and  $\delta = 17.19$ .

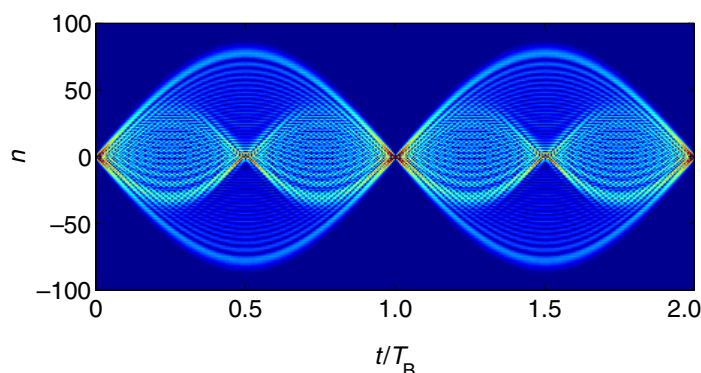


**Figure 7.** Dynamics of a breathing mode. The modulus of the wavefunction  $|\psi|$  is plotted versus ‘space’ and time. The parameters are  $\Delta = 80$ ,  $dF = 1$  and  $\delta = 6.734$ .

chosen as in figure 5, so that reconstruction happens again after integer multiples of  $T_{\text{BZ}} = T_{\text{B}}$ . One observes that the enveloping structure with the period  $T_{\text{BZ}} = T_{\text{B}}$  is overlayed by a breathing mode of smaller amplitude, which can be interpreted as a fraction of the wave packet remaining in one band all the time. Therefore the characteristic period of this part is  $T_1 = T_{\text{B}}/2$ . The gradient of the dispersion relation of a band changes at the edge of the Brillouin zone if there is no band transition. Therefore the direction of motion given by the group velocity changes after  $T_1 = T_{\text{B}}/2$  and the breathing amplitude of this part of the wave packet is thus smaller than the amplitude of the complete breathing mode.

Note that there is no systematic dispersion within the tight-binding approximation as long as the external field  $F$  is constant. This is obvious for reconstructing Bloch–Zener oscillations, i.e. commensurate periods  $T_1$  and  $T_2$ , since the initial wave packet reconstructs completely up to a global phase. In general, the dynamics is confined to a spatial interval of width  $\sqrt{\Delta^2 + \delta^2}$ ,



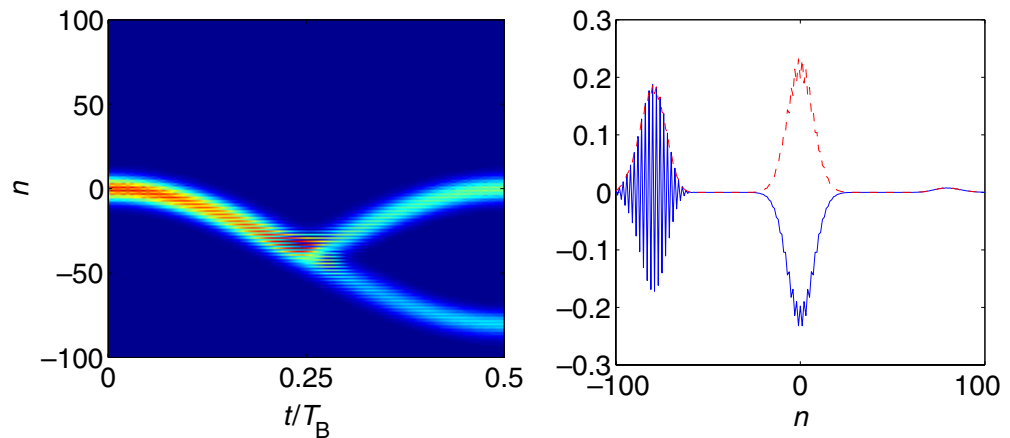


**Figure 8.** Splitting of a Gaussian wave packet in ‘space’. The left-hand side shows  $|\psi|^2$  versus ‘space’ and time. The right-hand side shows the absolute value (red dashed line) and the real part (blue solid line) of the wavefunction at  $t = 0.5 T_B$  versus ‘space’. The parameters are  $\Delta = 80$ ,  $dF = 1$  and  $\delta = 6.734$ .

due to the restriction to the two lowest minibands. Beyond these, decay must be taken into account. Fractions of the initial wave packet may tunnel to higher Bloch bands and finally escape to  $-\infty$ , leading to a pulsed output [23]. However, this decay is negligible for small  $F$ .

#### 4.5. Beam splitters

The Bloch–Zener transition between the two minibands can be used to construct a matter wave beam splitter with controllable ‘transmission’. To see this, note that interband transitions mainly take place at the edge of the Brillouin zone (see figure 2). In the case of a partial band transition, the wave packet is spatially separated, as illustrated in figure 5.

The time evolution of the squared modulus of a wave packet with a broad initial distribution  $\sim e^{-n^2/100}$  is shown in figure 8. At time  $t = 0.5 T_B$ , both parts of the wave packet have a Gaussian profile, but the lower part of the wavefunction consists of states with opposite momentum. Hence the phase of the wavefunction and therefore its real part oscillate strongly. Usually both parts merge again after a full Bloch period  $T_B$  (cf figure 5). However, a permanent splitting of the wave packet can be obtained by flipping the sign of  $F$  at  $t = 0.5 T_B$ , so that both parts of the wave packet are transported in opposite directions (compare [24]). This effect is shown in figure 9 (same initial state as above). After flipping the field  $F$ , the external force is constant and therefore the split wave packets continue their Bloch–Zener oscillations separately. Furthermore it is possible to control the occupation of each branch by the choice of  $\delta$ .

The transition probability at  $t = 0.5 T_B$  for a wave packet initially located in a single band is to good approximation given by the Landau–Zener formula (58). The numerical results for the occupation of the different branches (compare figure 8) at  $t = 0.5 T_B$  versus  $\delta$  are shown in figure 10. Such a controlled manipulation of the band gap can be achieved, for example, in optical lattices. In this case, it is also possible to construct a beam splitter in a different way, namely by ‘switching off’  $\delta$  completely at  $t = 0.5 T_B$ . Instead of Bloch–Zener oscillations, simple Bloch oscillations will appear with the advantage that the two wave packets can be separated

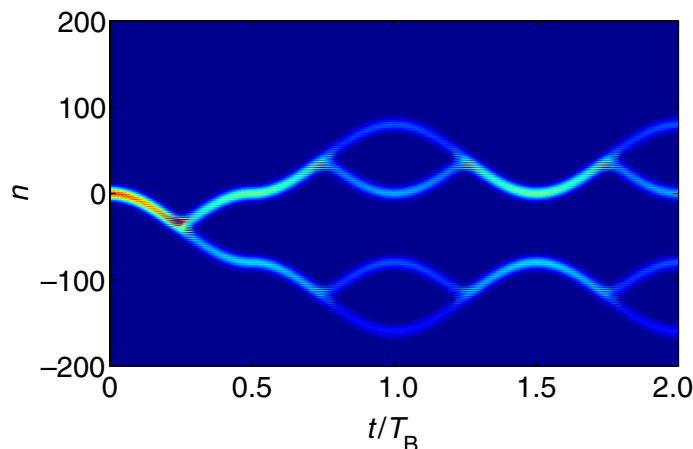


**Figure 9.** Splitting of a Gaussian wave packet in ‘real’ space. Shown is  $|\psi|^2$  versus ‘space’  $n$  and time  $t$ . The parameters are  $\Delta = 80$ ,  $d = 1$ ,  $\delta = 6.734$  and  $|F| = 1$ .

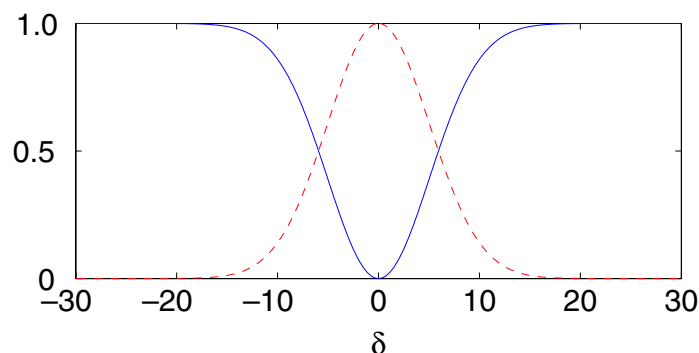


**Figure 10.** Occupation probability of the above Gaussian wave packet at  $t = 0.5 T_B$  versus  $\delta$ . The red dashed line shows the occupation in the interval  $-100 \leq n \leq -40$  whereas the blue solid line shows the occupation in the interval  $-41 \leq n \leq 20$ . The parameters are  $\Delta = 80$ ,  $d = 1$  and  $F = 1$ .

by low-loss transport as described in [12, 24]. In any case, it is possible to control the amplitude of each of the split wave packets by the choice of  $\delta$ .

## 5. Conclusion and outlook

In conclusion, we have investigated the interplay between Bloch oscillations and Zener tunnelling between the Bloch bands. To this end, we considered a particular tight-binding model under the influence of a static external field. This model satisfactorily describes the dynamics of a more realistic system, as demonstrated in a comparison with exact numerical computations [24]. An additional period-doubled potential leads to a splitting of the ground band into two minibands in the field-free case. For a nonzero external field, the spectrum of the system consists of exactly

two Wannier–Stark ladders. The dependence of the energy offset between the two ladders on the system parameters was discussed in detail.

The dynamics of the system is governed by two timescales, the Bloch period  $T_1$  defined in equation (71) and the period  $T_2$  of the Zener oscillation between the two energy ladders introduced in equation (72). If the two periods are commensurate, a wave packet will reconstruct periodically up to a global phase. The occupation of the two minibands at multiples of the Bloch period  $T_1$  oscillates sinusoidally in time. Furthermore, it was shown that the dynamics of the system can be reduced to a Whittaker–Hill differential equation. Unfortunately few analytic results are available for the solutions of this differential equation.

Finally some numerical examples of Bloch–Zener oscillations were given. It was shown that Bloch–Zener oscillations in a double-periodic potential can be used to construct matter wave beam splitters, e.g. for cold atoms in optical lattices.

A further important application of a Bloch–Zener oscillation as shown in figure 5 is the construction of a matter wave interferometer by introducing an additional external potential into one of the two branches of the split wave packet. Hence the band transitions can act as beam splitters in a Mach–Zehnder interferometer. Mach–Zehnder interferometry by repeated Landau–Zener tunnelling in the energy domain was previously discussed for different systems (see, e.g., [25, 26]). In contrast, Bloch–Zener oscillations also lead to a *spatial* separation of the two branches, which resembles the original Mach–Zehnder setup much more. These aspects will be discussed in more detail in a future publication [24].

## Acknowledgments

Support from the Deutsche Forschungsgemeinschaft via the Graduiertenkolleg ‘Nichtlineare Optik und Ultrakurzzeitphysik’ and the Studienstiftung des deutschen Volkes is gratefully acknowledged. We thank J R Anglin for valuable advice.

## Appendix

The time-independent Schrödinger equation in the basis of Bloch waves consists of two coupled differential equations (6) and (7). Using the ansatz

$$\langle \chi_{0,\kappa} | \Psi \rangle = Q_\kappa e^{-i\kappa E/F} \quad \text{and} \quad \langle \chi_{1,\kappa} | \Psi \rangle = P_\kappa e^{-i\kappa E/F}, \quad (\text{A.1})$$

we will show that in the case of a two band system there exist exactly two energy ladders. A similar proof can be found in [27] for a different system. Substituting (A.1) into equations (6) and (7), we obtain

$$\frac{\partial}{\partial \kappa} \begin{pmatrix} Q_\kappa \\ P_\kappa \end{pmatrix} = \frac{i}{F} \begin{pmatrix} E_{0,\kappa} - dF & M_\kappa^* \\ M_\kappa & E_{1,\kappa} \end{pmatrix} \begin{pmatrix} Q_\kappa \\ P_\kappa \end{pmatrix} = \mathbf{A}_\kappa \begin{pmatrix} Q_\kappa \\ P_\kappa \end{pmatrix}. \quad (\text{A.2})$$

The dispersion relations  $E_{0,\kappa}$ ,  $E_{1,\kappa}$  and the reduced transition matrix element  $M_\kappa$  are  $\pi/d$ -periodic. Therefore we can apply Floquet’s theorem, which says that a system of linear homogeneous differential equations with periodic coefficients as given above is solved by a

fundamental system of the structure

$$\mathbf{X}_\kappa = \mathbf{Y}_\kappa e^{i\kappa \mathbf{Z}}, \quad (\text{A.3})$$

where  $\mathbf{Y}_\kappa$  is a  $\pi/d$ -periodic  $(2 \times 2)$ -matrix and  $\mathbf{Z}$  is a constant complex  $(2 \times 2)$ -matrix. Let the eigenvalues of  $\mathbf{Z}$ , called characteristic exponents, be denoted by  $z_0$  and  $z_1$ . They are only defined up to multiples of  $2d$ . Multiplication of the fundamental system (A.3) with the eigenvectors of  $\mathbf{Z}$  from the right leads to

$$\begin{pmatrix} Q_{\kappa,n} \\ P_{\kappa,n} \end{pmatrix} = e^{i\kappa z_n} \begin{pmatrix} f_{\kappa,n} \\ g_{\kappa,n} \end{pmatrix}, \quad (\text{A.4})$$

with  $\pi/d$ -periodic functions  $f_{\kappa,n}$  and  $g_{\kappa,n}$ . Here,  $n = 0, 1$  distinguishes both possible eigenvectors. Because  $\langle \chi_{0,\kappa} | \Psi \rangle$  and  $\langle \chi_{1,\kappa} | \Psi \rangle$  have to be  $\pi/d$ -periodic, too, the phases are given by

$$-i\frac{\pi}{d}\frac{E}{F} + i\frac{\pi}{d}z_n = -i2\pi m, \quad (\text{A.5})$$

with  $m \in \mathbb{Z}$ . The energies are therefore

$$E_{n,m} = 2mdF + Fz_n. \quad (\text{A.6})$$

Obviously, there exist exactly two different energy ladders as long as the eigenvalues of  $\mathbf{Z}$  are distinct. Due to the fact that the Hamiltonian (1) is Hermitian, the energies  $E_{n,m}$ , and thus the  $z_n$ , are real numbers.

## References

- [1] Bloch F 1928 *Z. Phys.* **52** 555
- [2] Feldmann J, Leo K, Shah J, Miller B A B, Cunningham J E, Meier T, von Plessen G, Schulze A, Thomas P and Schmitt-Rink S 1992 *Phys. Rev. B* **46** 7252
- [3] Ben Dahan M, Peik E, Reichel J, Castin Y and Salomon C 1996 *Phys. Rev. Lett.* **76** 4508
- [4] Pertsch T, Dannberg P, Elfle W, Bräuer A and Lederer F 1999 *Phys. Rev. Lett.* **83** 4752
- [5] Morandotti R, Peschel U, Aitchinson J S, Eisenberg H S and Silberberg Y 1999 *Phys. Rev. Lett.* **83** 4756
- [6] Gutiérrez L, Díaz-de-Anda A, Flores J, Méndez-Sánchez R A, Monsivais G and Morales A 2006 in preparation
- [7] Zener C 1934 *Proc. R. Soc. Lond. A* **145** 523
- [8] Anderson B P and Kasevich M A 1998 *Science* **282** 1686
- [9] Rosam B, Leo K, Glück M, Keck F, Korsch H J, Zimmer F and Köhler K 2003 *Phys. Rev. B* **68** 125301
- [10] Trompeter H, Pertsch T, Lederer F, Michaelis D, Streppel U, Brauer A and Peschel U 2006 *Phys. Rev. Lett.* **96** 023901
- [11] Glück M, Kolovsky A R and Korsch H J 2002 *Phys. Rep.* **366** 103
- [12] Hartmann T, Keck F, Korsch H J and Mossmann S 2004 *New J. Phys.* **6** 2
- [13] Kovanis V I and Kenkre V M 1988 *Phys. Lett. A* **130** 147
- [14] Zhao X-G 1991 *J. Phys.: Condens. Matter* **3** 6021
- [15] Zhao X-G 1997 *J. Phys.: Condens. Matter* **9** L385
- [16] Kolovsky A R and Korsch H J 2003 *Phys. Rev. A* **67** 063601
- [17] Witthaut D, Keck F, Korsch H J and Mossmann S 2004 *New J. Phys.* **6** 41
- [18] Abramowitz M and Stegun I A 1972 *Handbook of Mathematical Functions* (New York: Dover)

- [19] Korsch H J and Mossmann S 2003 *Phys. Lett. A* **317** 54
- [20] Urwin K M and Arscott F M 1970 *Proc. R. Soc. Edinburgh* **69** 28
- [21] Landau L D 1932 *Phys. Z. Sowjet.* **1** 88
- [22] Zener C 1932 *Proc. R. Soc. Lond. A* **137** 696
- [23] Glück M, Keck F and Korsch H J 2002 *Phys. Rev. A* **66** 043418
- [24] Breid B M, Witthaut D and Korsch H J 2006 in preparation
- [25] Shimshoni E and Gefen Y 1991 *Ann. Phys.* **210** 16
- [26] Lubin D, Gefen Y and Goldhirsch I 1990 *Physica A* **168** 456
- [27] Fukuyama H, Bari R A and Fogedby H C 1973 *Phys. Rev. B* **8** 5579